Josephson vortex state across the phase diagram of $La_{2-x}Sr_xCuO_4$: A magneto-optics study

S. V. Dordevic*
Department of Physics, University of California, San Diego, La Jolla, California 92093, USA

Seiki Komiya and Yoichi Ando
Central Research Institute of Electric Power Industry, Tokyo, Japan

Y. J. Wang
National High Magnetic Field Laboratory, Tallahassee, Florida 32310, USA

D. N. Basov
Department of Physics, University of California, San Diego, La Jolla, California 92093, USA
(Received 23 May 2004; revised manuscript received 20 September 2004; published 7 February 2005)

We present a detailed doping dependent study of the Josephson vortex state in $La_{2-x}Sr_xCuO_4$ using infrared spectroscopy. A magnetic field as high as 17 tesla, applied along the CuO_2 planes, is found to suppress the Josephson plasmon in all measured samples. We find the strongest suppression in samples with dopings close to $x=1/8$ and attribute this effect to the spontaneous formation of in-plane charge inhomogenities at this doping level. Several theoretical models of the Josephson vortex state are applied to explain the observed effects.

DOI: 10.1103/PhysRevB.71.054503 PACS number(s): 74.72.−h, 74.25.Gz, 74.25.Qt

I. INTRODUCTION

The vortex state is one of the most generic and enigmatic states of matter.[1,2] Discovery of high-T_c cuprates opened another chapter in study of vortices in superconductors. Very high critical temperatures T_c and upper critical fields H_{c2} have allowed one to investigate parts of the *T-H* phase diagram that were previously unattainable. On the other hand these studies have had positive feedback on our understanding of many aspects of high-T_c superconductivity. Specifically, the electromagnetic response of vortices in cuprates has revealed a wealth of important information about the unusual superconducting state in these materials.[3]

In this paper we report on an infrared (IR) spectroscopy study of the interlayer ($\mathbf{E}\|c$) response of several well-characterized $La_{2-x}Sr_xCuO_4$ (LSCO) single crystals:[4] three underdoped with $x=0.10$, 0.12, and 0.125 (Ref. 5), an optimally doped with $x=0.15$, and two overdoped with $x=0.17$ (Ref. 5) and 0.20. These six samples map out the entire phase diagram, from underdoped to overdoped regimes, and provide a complete experimental picture of the Josephson vortex state in LSCO. All samples reveal a suppression of the *c*-axis superfluid density in the magnetic field. Field-induced modifications of the superfluid response in both under- and overdoped samples are generally in accord with the theories of the Josephson vortex dynamics. However, crystals with a doping level near $x=1/8$ reveal remarkably strong depression of the condensate inconsistent with the existing theoretical descriptions. We analyze other anomalies of the superconducting response in the vicinity of this doping level and conclude that weakening of superconductivity at $x=1/8$ may be triggered by quasistatic stripe order.

II. MAGNETO-OPTICAL EXPERIMENTS

The single crystals of LSCO studied in this work were grown using the TSFZ technique.[4,6] The crystallographic axes were determined by Laue analysis and then the samples were shaped into cylinders with the ac planes parallel to the basal plane. The samples were typically 5 mm in diameter and 2–3 mm thick. They have all been previously carefully characterized using magnetization, dc resisitivity and Hall measurements.[4,7]

The magneto-optical measurement consisted of two parts. First zero-field absolute reflectance $R(\omega)$ was collected over a broad frequency range, 10–48,000 cm^{-1}, from 6–7 K to room temperature. Second, field-induced changes were measured as $R(\omega,H,6\text{ K})/R(\omega,0\text{ T},6\text{ K})$, under zero field cooling conditions. The magnetic field was applied in Faraday geometry with $\mathbf{H}\|CuO_2$. In this geometry vortices penetrate in between the CuO_2 planes.[8] Figure 1(a) schematically displays a Josephson vortex sandwiched between two CuO_2 planes. The vortex is in the form of a cylinder whose base is a very elongated ellipse. The size of the vortex is determined by the in-plane λ_{ab} and out-of-plane λ_c penetration depths [Fig. 1(a)].

The optical conductivity $\sigma(\omega)=\sigma_1(\omega)+i\sigma_2(\omega)$ and the dielectric function $\epsilon(\omega)=\epsilon_1(\omega)+i\epsilon_2(\omega)$ were calculated from $R(\omega)$ using Kramers-Kronig analysis. In the superconducting state, the strength of the delta function in $\sigma_1(\omega)$, a so-called superfluid density ρ_s, is quantified with the plasma frequency $\omega_s^2=\rho_s=c^2/\lambda_c^2=4\pi e^2 n_s/m^*$ where n_s is the density of superconducting carriers and m^*, their effective mass. In order to accurately extract ω_s, a technique proposed by Dordevic *et al.*[9] was employed. The latter technique is capable of distinguishing screening due to the superconducting condensate from that of regular contribution associated with the response of unpaired carriers at $T<T_c$. Separation of those two components is essential when searching for small changes in the superfluid density as, for example, those induced by an external magnetic field. As expected, corrections were more

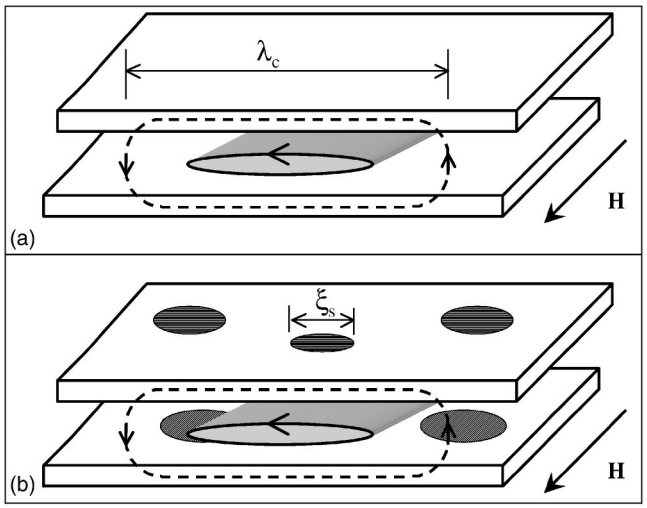

FIG. 1. (a) Josephson vortex sandwiched between two CuO_2 planes. (b) Josephson vortex between two CuO_2 planes with in-plane charge inhomogeneities. Note that the figure is not drawn to scale as the size of the patches ξ_s is typically 100–1000 times smaller than the vortex size λ_c (Table I).

important for samples with higher dopings because the regular contribution was greater there.

Figure 2 displays reflectance data for $x=0.125$ LSCO sample over an extended frequency interval. In the normal state, above T_c, the low-frequency reflectance is featureless, with absolute values near 50%. At $\omega \to 0$, there is a slight upturn toward $R \sim 1$. At higher frequencies ($100 \lesssim \omega \lesssim 700$ cm^{-1}), the spectrum is dominated by optically active phonons. Above 700 cm^{-1}, the reflectance is again featureless with low absolute values ($R \sim 15\%$). In the superconducting state the reflectance acquires a characteristic shape of a plasma edge,[10] which is usually described by a so called two-fluid model, commonly used in the microwave and IR frequency ranges:[11–13]

$$\epsilon(\omega) = \epsilon_\infty - \frac{\omega_s^2}{\omega^2} - \frac{\omega_n^2}{\omega^2 + i\gamma_{sr}\omega}, \qquad (1)$$

where ϵ_∞ is the high-frequency dielectric function and ω_n and γ_{sr} are the regular component plasma frequency and scattering rate. A plasma edge develops approximately at the frequency $\omega_s/\sqrt{\epsilon_\infty}$. As temperature decreases the plasma edge sharpens and moves to higher frequencies, which indicates an increase in ω_s.

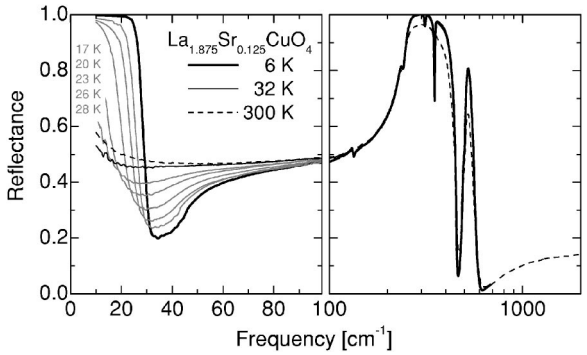

FIG. 2. Temperature dependence of infrared reflectance $R(\omega, T, H=0\ \mathrm{T})$ for the $x=0.125$ LSCO sample. Note that the frequency scale changes from linear to logarithmic above 100 cm^{-1}.

Figure 3 presents the temperature dependence of reflectance $R(\omega, T, H=0\ \mathrm{T})$ for all six samples used in this magneto-optical study. In addition the reflectance of $x=0.08$ and another 0.125 sample, for which no high field data have been obtained, are also shown. Only the reflectance below the phonon region is displayed for clarity. For all samples, horizontal axes are shown in both the absolute ω and relative units ω/ω_0, where ω_0 is the frequency of the plasma edge. Note that in the $x=0.08$ sample the plasma edge can be observed only at the lowest temperatures; at higher temperatures the edge moves outside the low energy cutoff of our measurements: $\omega \lesssim 10$ cm^{-1}.

Figure 4 presents the relative suppression of the superfluid plasma frequency $\omega_s(T)/\omega_s(6\ \mathrm{K})$, extracted using a procedure described in Ref. 9, as a function of reduced temperature T/T_c. The values of critical temperatures T_c and the superfluid plasma frequencies at the lowest temperature $\omega_s(6\ \mathrm{K})$ are summarized in Table I. As mentioned above, for the 8% sample a plasma edge can be observed only at the lowest measured temperature. The values of $\omega_s(T)$ at intermediate temperatures (gray points) are only rough estimates based on the fits of reflectance at higher frequencies ($\omega \gtrsim 10$ cm^{-1}). In all other samples, the superfluid plasma frequency is suppressed rapidly as temperature increases, behavior characteristic of systems with *d*-wave symmetry of the order parameter.[12,14]

Figure 5 displays magnetic field dependence of reflectance $R(\omega, H, T=6\ \mathrm{K})$ in the Josephson plasmon region. We do not observe any additional modes in the presence of the field in any of the samples. This is in contrast to the behavior of double-layered systems, where new resonances are observed both in the case of pancake vortices[15] and Josephson vortices.[16] In all LSCO samples, as the field increases the plasma minimum broadens and the plasma edge shifts to lower frequencies. This latter effect indicates a reduction of ω_s consistent with the notion of destruction of the superfluid by the magnetic field. However, in no samples is the 17 T field sufficient to completely destroy superconductivity, and the characteristic reflectance edges are still observed in all $R(\omega, H=17\ \mathrm{T}, T=6\ \mathrm{K})$ curves. This is not unexpected, as the upper critical field H_{c2} for fields oriented parallel to the CuO_2 planes is beyond what can be achieved in laboratories today.[17] Figure 6 presents the relative change of the superfluid plasma frequency $\omega_s(H)/\omega_s(0\ \mathrm{T})$ with magnetic field H. The smallest relative suppression of only 15% at 17 T is observed in overdoped samples $x=0.17$ and 0.20. The suppression becomes somewhat stronger at optimal doping: 25% in 0.15 sample. The magnitude of $\omega_s(17\ \mathrm{T})/\omega_s(0\ \mathrm{T})$ is approaching 40% in 0.125 sample exceeding that of $x=0.1$ and 0.12 materials where $\omega_s(17\ \mathrm{T})/\omega_s(0\ \mathrm{T}) \simeq 30\%$. Apart from difference in the overall strength of the superfluid density depression, the functional form of $\omega_s(H)/\omega_s(0\ \mathrm{T})$ traces is also different. Indeed, we find the downward curvature in $x=0.125$ and, to a lesser extent, 0.12 sample. All other samples show an upward curvature.

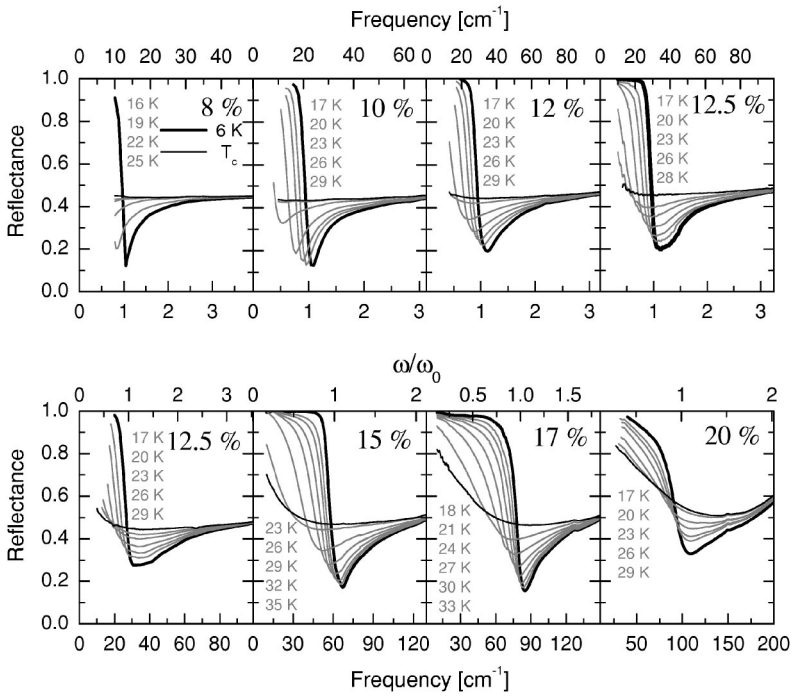

FIG. 3. Temperature dependence of infrared reflectance $R(\omega,T,H=0\ \mathrm{T})$ for all LSCO samples. Only spectra taken at temperatures below T_c are shown for clarity. Both absolute ω and relative frequency units ω/ω_0 are shown; ω_0 is the frequency of the plasma minimum at 6–7 K (Table I).

III. THEORETICAL MODELS

Several theoretical models have been proposed to describe the electrodynamic response of a layered superconductor in the presence of external magnetic field parallel to the planes.[8,18–27] Some of these theories permit explicit comparison with the experimental results presented in this work because they deliver expressions for the frequency dependence of optical constants in magnetic field and/or prescribe a specific form for the field dependence of the superfluid density. In the latter group we find models proposed by Bulaevskii *et al.*,[19,20] Coffey and Clam;[21–23] Tachiki, Koyama, and Takahashi,[8] and Won, Jang, and Maki.[24,25] These models have been frequently applied to the analysis of experimental data, typically for $H<7$ T (Refs. 28–31). For convenience we briefly overview these models before comparing predictions with experimental data.

A. Field-induced phase difference and superfluid density

The model by Bulaevskii *et al.*[19] allows one to access the impact of the applied magnetic field on the phase difference between the CuO_2 planes. The model delivers a simple formula for the field dependence of the superconducting plasma frequency with no adjustable parameters,

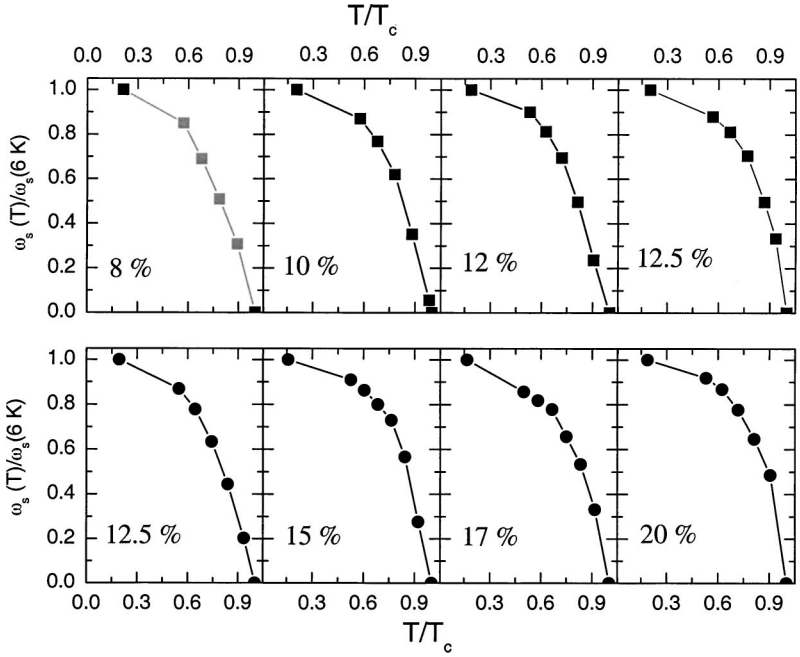

FIG. 4. Temperature dependence of the superfluid plasma frequency in zero field $\omega_s(T)/\omega_s(6\ \mathrm{K})$. $\omega_s(6\ \mathrm{K})$ values are reported in Table I.

TABLE I. Parameters of $La_{2-x}Sr_xCuO_4$ (LSCO) samples discussed in this work: superconducting critical temperature T_c, DC conductivity at T_c σ_{DC}, superconducting plasma frequency at 6 K ω_s, *c*-axis penetration depth λ_c, in-plane penetration depth λ_{ab} from both IR[39–41] and μSR measurements,[51] anisotropy ratio $\gamma=\lambda_c/\lambda_{ab}$ and the Josephson length $\lambda_J=\gamma d$ ($d=6.61$ Å). The table also includes the values of characteristic field H_0 [Eq. (2)], viscosity coefficient η [Eq. (5)], vortex mass M [Eq. (6)], and the best fits of the pinning constant κ_p [Eq. (7)] with $M=0$ and $M\neq 0$. The last three rows are the frequency of the plasma edge ω_0, and the fitting parameters ω_n and ω_s^{fit} from Eq. (1) (Ref. 43).

	0.08	0.10	0.12	0.125	0.125	0.15	0.17	0.20
T_c [K]	28	32	32	32	32	38	36	32
σ_{DC} [Ω^{-1} cm^{-1}]	0.35	1	2.8	6.5	4	12.8	32	95
ω_s [cm^{-1}]	64	110	160	159	153	344	360	515
λ_c [μm]	24.2	14	9.7	9.7	10.1	4.5	4.3	3
λ_{ab} [μm]-IR	0.6				0.63		0.346	
γ-IR	40				16		12.4	
λ_J [μm]-IR	265				106		82	
λ_c [μm]-μSR	9.2	6				3.9	3.1	2.3
λ_{ab} [μm]-μSR	0.38	0.29			0.33	0.25	0.22	0.19
γ-μSR	24.2	20.7				15.6	14.1	12.1
λ_J [μm]-μSR	160	137				103	93	80
H_0[T]	18.6	24.5	39.3	40.5	38.8	66	60.7	75
C_1 [Pa/T]	2.8	8.4	17.4	17.4	16	81	89	182
η [Pa cm]	0.09	0.34	1.5	3.6	2.1	11.6	26.8	98.3
M [Pa cm^2]	2.43	3.18	5.12	5.27	5.05	8.58	7.93	9.78
κ_p M=0 [Pa]		140	280	180		1800	5500	8000
κ_p (M$\neq$0) [Pa]		140	280	185		1850	5700	8100
ω_0 [cm^{-1}]	12.5	22	31	30.5	28	61	81	99
ω_s^{fit} [cm^{-1}]	65	115	155	160	150	320	418	550
ω_n [cm^{-1}]	390	550	500	800	800	800	1150	2200

$$\omega_s(H)=\omega_s(0T)\left(1-\frac{\pi}{8}\frac{H}{H_0}\ln\frac{H_0}{H}\right). \tag{2}$$

As can be seen from Eq. (2), the suppression of superfluid density by magnetic field depends only on the characteristic field $H_0=\Phi_0/\gamma s^2$. In this expression, Φ_0 is the flux quantum, $\gamma=\lambda_c/\lambda_{ab}$ is the anisotropy factor, and $s\simeq 0.66$ nm is the CuO_2 interlayer distance in LSCO.[32] The characteristic field H_0 is therefore inversely proportional to the anisotropy factor γ, which also quantifies the strength of the coupling between the CuO_2 layers. The values of H_0, λ_c, λ_{ab}, and γ for all the samples are given in Table I. As can be seen from Fig. 7, the model provides a satisfactory account of the data for $H/H_0 \lesssim 0.3$ for 0.10, 0.15, 0.17, and 0.20 doping levels. However, the model is not appropriate for either $x=0.12$ or 0.125 samples because the curvature of the model dependence is opposite to the one observed experimentally.

After Eq. (2) had been published,[19] it was realized by the authors themselves[20] that one of the assumptions of their model, $\omega_s^2\propto\langle\cos\theta\rangle$, (valid for long Josephson junctions) cannot directly be applied to layered superconductors. In the latter expression, θ is the phase difference between neighboring CuO_2 planes and $\langle\ldots\rangle$ denotes a spatial average. A correct theory for layered superconductors was developed,[20] however, no new analytical expression has been given. Based on our results it appears that the assumption $\omega_s^2\propto\langle\cos\theta\rangle$ might also be valid in layered superconductors in the limit $H/H_0\rightarrow 0$, for doping levels different from $x\simeq 1/8$.

B. Dynamics of Josephson vortices and superfluid density

The CC and TKT models approach the problem of Josephson vortex state from a different prospective than Bulaevskii *et al.*[19] Both TKT and CC theories are based on a simple phenomenological description of vortex dynamics.[33,34] The equation of vortex motion under the influence of Lorentz force caused by current $\vec{\mathbf{J}}$ is

$$M\ddot{u}+\eta\dot{u}+\kappa_p u=\frac{\Phi_0}{c}\vec{\mathbf{J}}\times\vec{n}, \tag{3}$$

where M is the vortex inertial mass, η is the viscous force coefficient, κ_p is the vortex pinning force (Labusch) constant, Φ_0 is the flux quantum, $\vec{n}$ is the unit vector in the direction of the vortex, and $u(t)$ is the vortex displacement from its equilibrium (pinned) position.

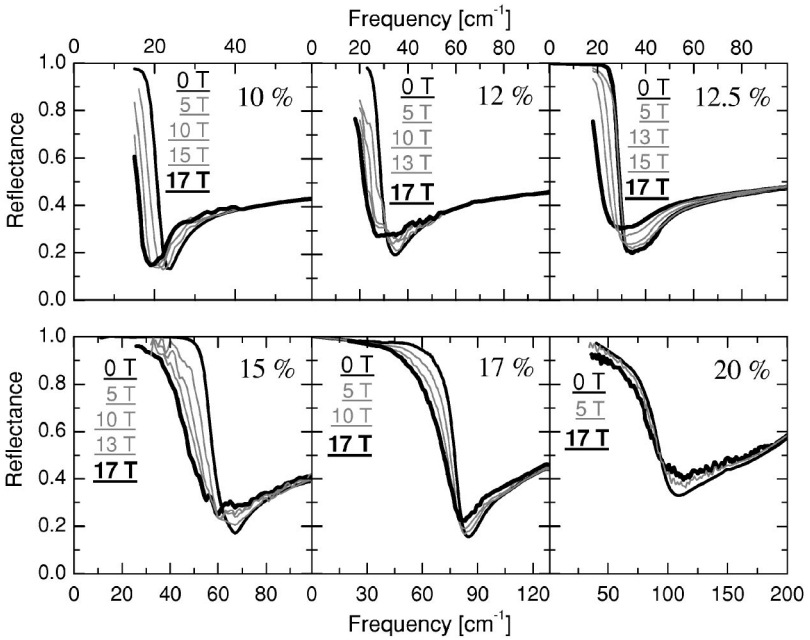

FIG. 5. Magnetic field dependence of infrared reflectance $R(\omega, T=6\ \mathrm{K}, H)$. For each sample only a few in-field spectra are shown for clarity.

The CC model delivers an expression for the complex penetration depth $\tilde{\lambda}(\omega, T, H)$ in terms of the normal skin depth $\delta_{nf}=\sqrt{2\rho_{nf}/\mu_0\omega}$ ($\rho_{nf}=1/\sigma_{nf}$ is the normal fluid resistivity) and the complex skin depth arising from both the vortex motion and flux creep δ_{vc} [Eq. (4) from Ref. 23],

$$\tilde{\lambda}(\omega,H,T)=\sqrt{\frac{\lambda^2(H,T)-\frac{i}{2}\tilde{\delta}_{vc}^2(\omega,H,T)}{1+\frac{2i\lambda^2(H,T)}{\delta_{nf}^2(H,T,\omega)}}}. \qquad (4)$$

This is a general equation that applies to all Type-II superconductors, and we assume that it also holds for high-T_c cuprates, in particular, for the c-axis penetration depth. At sufficiently low temperatures, the effects associated with flux creep can be neglected and the skin depth reduces to $\delta_{vc}=\sqrt{2\phi_0 H\mu/\mu_0\omega}$, where $\tilde{\mu}=(1-i\kappa_p/\eta\omega)^{-1}\mu^{-1}$ is the complex dynamical vortex mobility. It can be easily shown that in this case Eq. (4) reduces to the TKT expression [see Eq. (7) below].

Starting with Eq. (3), the CC model allows one to estimate several important parameters of vortex dynamics, such as the viscosity coefficient η and vortex mass M. The viscosity coefficient η is given by the following formula [Eq. (5.7) from Ref. 21]:

$$\eta=0.354\,3\frac{1}{\gamma}\frac{\sigma_{DC}\phi_0^2}{s^2c^2}, \qquad (5)$$

where σ_{dc} is the dc conductivity and c is the speed of light. The vortex mass M within the CC model is given by the formula [Eq. (16) from Ref. 22],

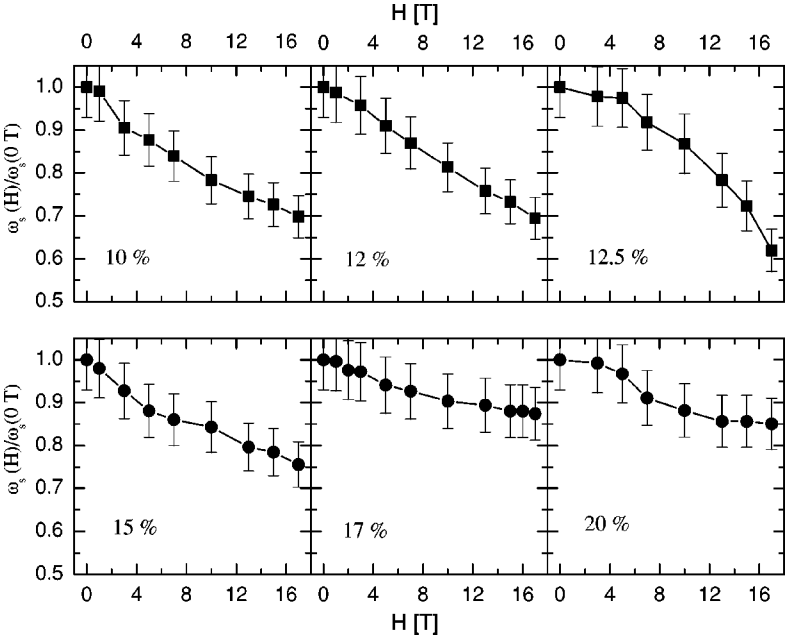

FIG. 6. Magnetic field dependence of the superfluid plasma frequency at 6 K $\omega_s(H)/\omega_s(0T)$.

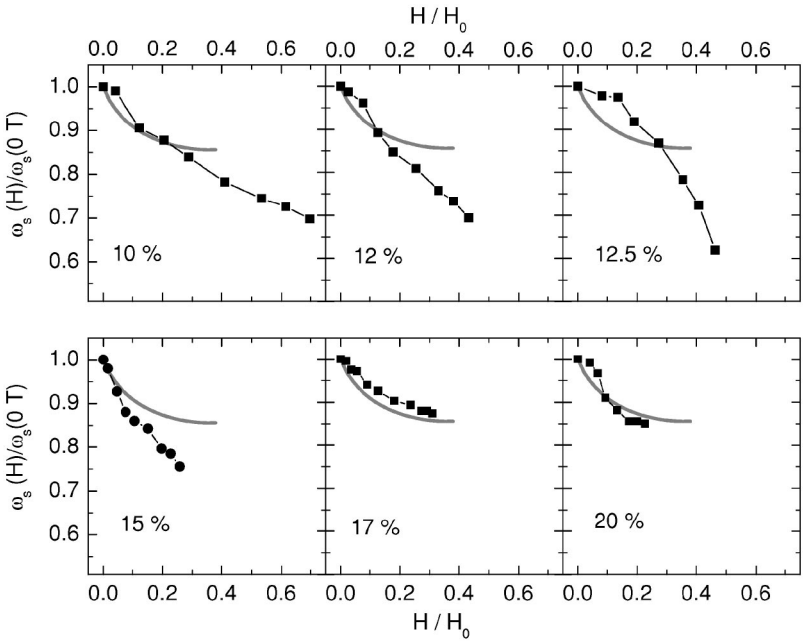

FIG. 7. The model of Bulaevskii *et al.*[19] applied to our $\omega_s(H)/\omega_s(6\ \mathrm{K})$ data. Apart from $x \sim 1/8$ doping the model provides a satisfactory account of the data below $H/H_0 < 0.3$; the model breaks down at higher fields.

$$M \simeq \frac{\Phi_0^2}{4\pi}\frac{1}{\gamma}\frac{1}{\bar{c}^2 d_i s}, \tag{6}$$

where d_i is the thickness of insulating layers and $\bar{c}$ is the speed of light in the insulating layers. The values of both the mass and viscosity calculated using CC formulas are given in Table I and are used when fitting the experimental data with Eq. (4), or equivalently with the TKT expression Eq. (7).

Similar to CC, the TKT model addresses the issue of the Josephson plasmon in the mixed state. An expression for the dielectric function $\epsilon(\omega)$ applicable at low temperatures and for frequencies $\omega \ll \omega_s$ has been derived,

$$\epsilon(\omega) = \epsilon_\infty - \frac{\dfrac{\omega_s^2}{\omega^2} + \dfrac{\omega_n^2}{\omega^2 + i\gamma_{sr}\omega}}{1 + \dfrac{\phi_0}{4\pi\lambda_c^2}\dfrac{H}{\kappa_p - i\eta\omega - M\omega^2}}, \tag{7}$$

For $H=0$, Eq. (7) reduces to the well-known "two-fluid" formula [Eq. (1)]. As mentioned above, the CC expression for the complex penetration depth $\tilde{\lambda}$ [Eq. (4)], i.e., dielectric constant $\epsilon(\omega) = \epsilon_\infty - c^2/(\omega^2\tilde{\lambda}^2)$, reduces to the TKT expression at low temperatures.

In order to compare predictions of the TKT model with the data, we have first fitted the zero field reflectance with a two-fluid model [Eq. (1)]. This procedure yielded ω_s^{fit} and ω_n (γ_{sr} was assumed to be 5000 cm^{-1} for all samples), as reported in Table I. The values of η and M were estimated from CC formulas, Eqs. (5) and (6), respectively. The only unknown parameter remaining in Eq. (7) is the pinning constant κ_p. We have numerically solved Eq. (7) for $\omega_s(H)$, in the limit $\omega \to 0$. The values of κ that produced the best fits are given in Table I. As can be seen from Fig. 8, very good fits can be obtained for all samples except for $x=0.12$ and 0.125 crystals. Particularly poor is the fit for the $x=0.125$ sample. The failure of both Bulaevskii and TKT/CC models to account for the experimental data in magnetic field at $x=1/8$ crystal indicates that the properties of superconducting condensate in this doping regime are fundamentally different from other samples on either under- or overdoped sides of the phase diagram.

C. Zeeman effect

Interplay of the Zeeman effect with superconductivity has been discussed is several publications in the early 1960s[35,36] and, more recently, in the context of high-field behavior of cuprates.[24–27] Intuitively, the Zeeman effect is expected to be more pronounced in *d*-wave superconductors, including cuprates. In conventional *s*-wave layered superconductors, when the field is applied along the planes, the pair-breaking effect is negligible for fields smaller than the gap (see Fig. 9, left panel). However, in cuprates *d*-wave symmetry of the order parameter implies points on the Fermi surface where the gap goes to zero, in which case *any* magnetic field can cause pair breaking. When the maximum gap is large compared to the applied field (Fig. 9, middle panel), relatively small pockets of the Fermi surface around the nodal points are affected and the pair-breaking effect is almost negligible. If that is the case, then the suppression of the superfluid is primarily due to vortex motion. However, if the magnitude of the gap is comparable to the applied magnetic field (Fig. 9, right panel), then larger portions of the Fermi surface become affected. In this case direct pair-breaking effects and vortex-dynamics effects have to be treated on equal footing when field-induced modification of the superfluid density is considered.

Won, Jang, and Maki[24,25] derived an expression for the suppression of the superfluid density in parallel field due to the Zeeman effect,

$$\frac{\omega_s^2(H)}{\omega_s^2(0)} = \sqrt{1 - \left(\frac{H}{\Delta}\right)^2}, \tag{8}$$

where Δ is the superconduting gap. Equation (8) produces a characteristic downward curvature of $\omega_s(H)$ traces, opposite

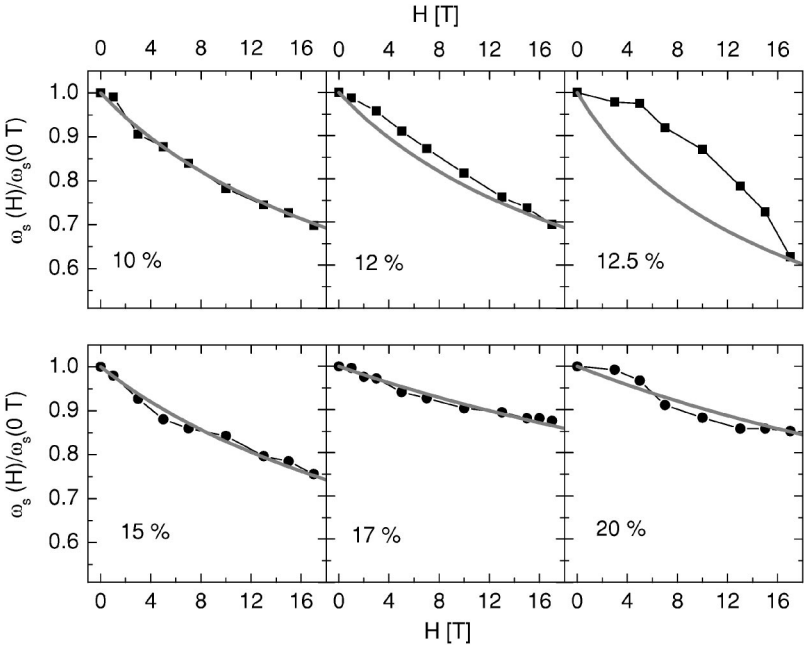

FIG. 8. The models of Coffey and Clam[21–23] (CC) and Tachiki, Koyama, and Takahashi[8] (TKT) applied to our $\omega_s(H)/\omega_s(6\ \mathrm{K})$ data. These models reproduce the data for all samples, except for $x\sim 1/8$ doping. Moreover, for dopings different from $1/8$ the model yields physically realistic values of the parameters, such as the viscosity coefficient η and the pinning constant κ_p (Table I).

to that of the models by Bulaevskii *et al.*, TKT, and CC. In Fig. 10, we display the data for the $x=0.125$ sample along with the fit using Eq. (8) (gray line). The fit can, in principle, reproduce the observed behavior.

A drawback of the formalism behind Eq. (8) is that it ignores suppression of the superfluid density because of the vortex motion. In order to account for both vortex dynamics and Zeeman pair breaking we have naively assumed that the two processes are independent and additive. As an example in Fig. 10 we also fit the data for the $x=0.125$ sample by assigning 50% of superfluid suppression to pair breaking (Eq. (8)) and the other 50% to vortex dynamics [Eq. (7)]. The result of the fit is shown in Fig. 10 with a thick line, along with each of individual components (dotted and dashed lines). The fit is better compared to the one based on Eq. (8) alone. The best fit is obtained when the magnitude of $2\Delta\simeq 35\ \mathrm{cm}^{-1}$. As we discuss below, this result is supported by direct measurements of the *ab*-plane conductivity in the same specimen. We stress that the downward curvature in the field dependence of the superfluid density can be taken as an indicator of the prominence of direct pair breaking in the system. Since this effect is amplified if superconducting gap is depressed, we conclude that $x=1/8$ doping is characterized by strong depletion of the 2Δ value.

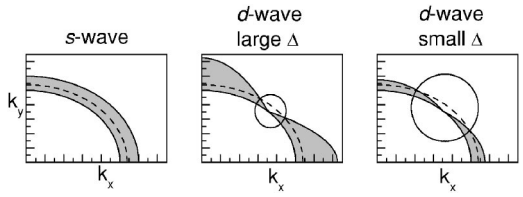

FIG. 9. Field-induced pair-breaking effects in *s*-wave and *d*-wave superconductors. Left panel: for *s*-wave gap (shaded region), small magnetic field (dashed line) is ineffective in pair breaking until its magnitude exceeds the gap value. Middle and right panels: for superconductors with *d*-wave symmetry of the order parameter, the gap value goes to zero at the so-called nodal points and any finite field can cause pair breaking. However, when the maximum gap (at $[0,\pi]$, $[\pi,0]$, and symmetry related points) is small, a larger portion of the Fermi surface is influenced by the field (circled region) and the impact of the field is enhanced. The latter situation is relevant to LSCO samples with dopings close to $x=1/8$.

IV. DISCUSSION

The bottom panel of Fig. 11 summarizes the doping dependence of the relative superfluid suppression at 17 T: $\omega_s(17\ \mathrm{T})/\omega_s(0\ \mathrm{T})$. The curve displays a dip at $x=1/8$, and we will try here to elucidate possible origins of

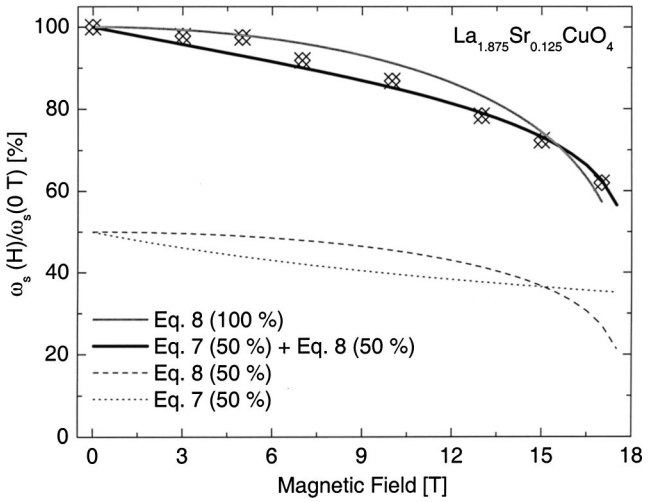

FIG. 10. Won, Jang, and Maki's model[24,25] combined with the TKT and applied to 0.125 data, as described in the text. Also shown are individual components that are set to produce equal contribution to a net suppression of superfluid plasma frequency. Gray line illustrates the Zeeman effect alone [Eq. (8)].

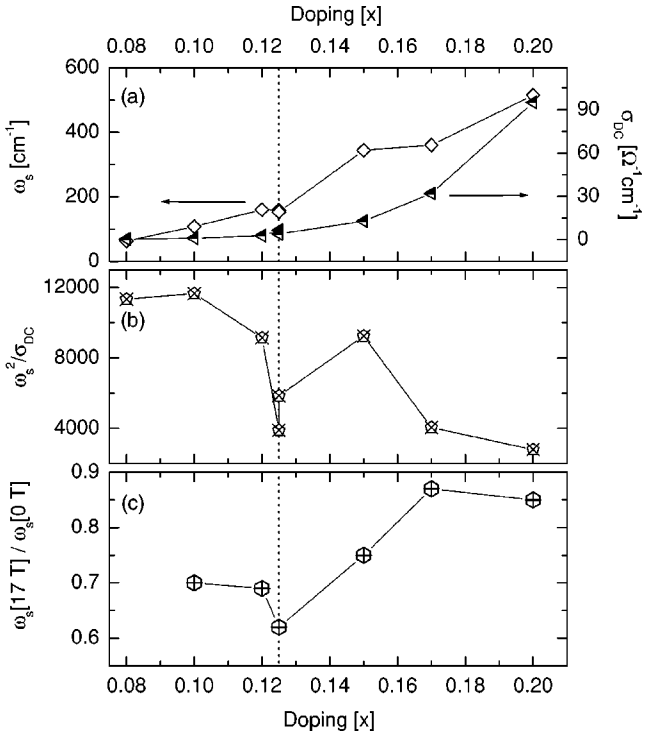

FIG. 11. Doping dependence of the superfluid plasma frequency ω_s [panel (a), left axis], DC conductivity at T_c σ_{dc} [panel (a), right axis], the ratio ω_s^2/σ_{dc} [panel (b)], and of the suppression of the superfluid plasma frequency at 17 T $\omega_s(17\ \mathrm{T})/\omega_s(0\ \mathrm{T})$ [panel (c)]. Anomalous behavior near $x=1/8$ is attributed to inhomogeneous superconducting state, as described in the text.

this anomaly. In the top panel of Fig. 11, we present the doping dependence of the superfluid plasma frequency ω_s(6 K) (at 0 T) and dc conductivity at T_c σ_{dc}. These two quantities reveal only minor anomalies at 1/8 doping (see also Table I). However the ratio ω_s^2/σ_{dc}, shown in the middle panel displays a pronounced dip at $x=1/8$. In the dirty limit BCS theory, the latter quantity is given by,[37]

$$\frac{\omega_s^2}{\sigma_{dc}} = 4\pi^2\Delta, \tag{9}$$

where 2Δ is the superconducting energy gap. This simple relation is shown to be followed by layered superconductors, including cuprates and also transition metal dicalchogenides and organics.[9,38] The middle panel of Fig. 11 will allow us to examine more closely the relation (9) in LSCO family. Apparently the magnitude of the energy scale relevant for superconductivity extracted from the scaling relation in Fig. 11 appears to be suppressed at $x=1/8$. This result has been anticipated above based on Eq. (8). IR measurements of the in-plane response of the same $x=0.125$ LSCO crystal[39] have shown that the superfluid density is collected from the frequency range below 70–80 cm^{-1}. This sets up the upper bound for the magnitude of 2Δ, whereas the analysis of the $1/\tau(\omega)$ suggests that the gap value can be as small as 40 cm^{-1} (Ref. 39). Preliminary results on LSCO crystals with both lower $x=0.08$ (Ref. 40) and higher dopings $x=0.17$ (Ref. 41) indicate that the energy scales from which the condensate is collected in these latter samples are broader than at $x=0.125$. These experimental findings are in accord with the nonmonotonic doping dependence of ω_s^2/σ_{dc}, as displayed in the middle panel of Fig. 11.

When searching for the possible origins of anomalous sensitivity of superfluid to magnetic field at $x\simeq 1/8$ doping, it is imperative to consider the effects of intrinsic in-plane charge inhomogeneities. Theoretical models of lightly doped Mott-Hubbard insulators have predicted spontaneous spin and charge self-organization on diverse length scales.[42] It has recently been demonstrated that *c*-axis IR measurements can be used to monitor the formation of in-plane inhomogeneities in the cuprates.[43] The method is based on the effect these inhomogeneities have on the line shape of the Josephson plasmon in the *c*-axis loss function. The study has established that the superconducting condensate is highly inhomogenious. In combination with μSR and NMR results,[44–46] IR analysis has revealed the existence of regions (patches) within CuO_2 planes within which the superconducitivity is either weakened or completely destroyed.[47] The effect of phase segregation is observed to be strongest at $x=1/8$ and decreases at both higher and lower dopings.[43] The size of the patches can be estimated from neutron-scattering measurements, which have reported the correlation length ξ_s of static spin correlations of at least 200 Å at $x\simeq 1/8$ (Refs. 48 and 49). We argue that these in-plane charge inhomogeneities are also responsible for anomalous sensitivity of the superconducting condensate to external magnetic field at 1/8 doping. Figure 1(a) schematically displays a situation when inhomogeneities are absent. In this homogeneous case, circulating supercurrents flow through fully superconducting CuO_2 planes; between the planes the current is of the Josephson type (hence, the name "Josephson vortex"). In the presence of in-plane charge inhomogeneities [Fig. 1(b)], vortex currents must close the loop through magnetically ordered (probably nonsuperconducting)[50] regions. At $x=1/8$ doping, where the density and size of the patches is biggest, there is a significant number of vortex filaments whose in-plane currents are affected. Moreover, the patches are intuitively expected to influence the vortex dynamics and, consequently, the suppression of superfluid. Alternatively, one can envision that the in-plane charge inhomogeneities weaken the *average* Josephson coupling, making it more sensible to magnetic field. All these effects require further theoretical consideration.

V. SUMMARY

Our magneto-optical results have revealed anomalous sensitivity of superconducting state in LSCO to external magnetic field around 1/8 doping. We have shown that the origins of this effect are twofold. On the one hand, the value of the superconducting gap is depleted at $x=1/8$, which makes the Zeeman effects (direct pair breaking) more prominent. On the other hand, the presence of in-plane charge inhomogeneities at 1/8 doping affects the vortex dynamics and/or the average strength of Josephson coupling. Both of these effects weaken the superconductivity at around 1/8 doping, making it more vulnerable to the applied magnetic field.

ACKNOWLEDGMENTS

The research supported by NSF, DoE, and the Research Corporation. A portion of the work was performed at the NHMFL, which is supported by NSF Cooperative Agreement No. DMR-0084173 and by the State of Florida. We thank L. Bulaevskii, S.A. Kivelson, K. Maki, and H. Won for useful discussions.

*Present address: Department of Physics, Brookhaven National Laboratory, Upton, NY 11973, USA.

[1] P. G. Saffman, *Vortex dynamics* (Cambridge University Press, 1992).
[2] G. W. Crabtree and D. R. Nelson, Phys. Today **50**, 38, (1997).
[3] G. Blatter, M. V. Feigel'man, V. B. Geshkenbein, A. I. Larkin, and V. M. Vinokur, Rev. Mod. Phys. **66**, 1125 (1994), and references therein.
[4] Y. Ando, A. N. Lavrov, S. Komiya, K. Segawa, and X. F. Sun, Phys. Rev. Lett. **87**, 017001 (2001).
[5] S. V. Dordevic, Seiki Komiya, Yoichi Ando, Y. J. Wang, and D. N. Basov, Europhys. Lett. **61**, 122 (2003).
[6] Seiki Komiya, Yoichi Ando, X. F. Sun, and A. N. Lavrov, Phys. Rev. B **65**, 214535 (2002).
[7] Yoichi Ando, Y. Kurita, Seiki Komiya, S. Ono, and Kouji Segawa, cond-mat/0401034 (unpublished).
[8] M. Tachiki, T. Koyama, and S. Takahashi, Phys. Rev. B **50**, 7065 (1994).
[9] S. V. Dordevic, E. J. Singley, D. N. Basov, Seiki Komiya, Yoichi Ando, E. Bucher, C. C. Homes, and M. Strongin, Phys. Rev. B **65**, 134511 (2002).
[10] S. Uchida, K. Tamasaku, and S. Tajima, Phys. Rev. B **53**, 14 558 (1996).
[11] A. Hosseini, R. Harris, Saeid Kamal, P. Dosanjh, J. Preston, Ruixing Liang, W. N. Hardy, and D. A. Bonn, Phys. Rev. B **60**, 1349 (1999).
[12] D. A. Bonn and W. N. Hardy, in *Physical Properties of High-T_c Superconductors*, Vol. V, edited by D. M. Ginsberg (World Scientific, Singapore, 1996).
[13] D. B. Tanner and T. Timusk, in *Physical Properties of High Temperature Superconductors III*, edited by D. M. Ginsberg (World Scientific, Singapore, 1993), and references therein.
[14] C. Panagopoulos, J. R. Cooper, T. Xiang, Y. S. Wang, and C. W. Chu, Phys. Rev. B **61**, R3808 (2000).
[15] H.-T. S. Lihn, S. Wu, H. D. Drew, S. Kaplan, Qi Li, and D. B. Fenner, Phys. Rev. Lett. **76**, 3810 (1996).
[16] K. M. Kojima, S. Uchida, Y. Fudamoto, and S. Tajima, Phys. Rev. Lett. **89**, 247001 (2002).
[17] G. Boebinger, Phys. Today **49**, 36 (1996).
[18] L. N. Bulaevskii, Sov. Phys. JETP **37**, 1133 (1973).
[19] L. N. Bulaevskii, M. P. Maley, and M. Tachiki, Phys. Rev. Lett. **74**, 801 (1995).
[20] L. N. Bulaevskii, D. Dominguez, M. P. Maley, and A. R. Bishop, Phys. Rev. B **55**, 8482 (1997).
[21] J. R. Clem and M. W. Coffey, Phys. Rev. B **42**, 6209 (1990).
[22] M. W. Coffey and J. R. Clem, Phys. Rev. B **44**, 6903 (1991).
[23] M. W. Coffey and J. R. Clem, Phys. Rev. Lett. **67**, 386 (1991).
[24] H. Won, H. Jang, and K. Maki, cond-mat/9901252.
[25] H. Won, H. Jang, and K. Maki, Physica B **281-282**, 944 (2000).
[26] K. Yang and S. L. Sondhi, Phys. Rev. B **57**, 8566 (1998).
[27] K. Yang and S. L. Sondhi, J. Appl. Phys. **87**, 5549 (2000).
[28] M. Golosovsky, M. Tsindlekht, and D. Davidov, Supercond. Sci. Technol. **9**, 1 (1996), and references therein.
[29] A. A. Pesetski and T. R. Lemberger, Phys. Rev. B **62**, 11 826 (2000).
[30] A. M. Gerrits, M. E. J. Boonman, A. Wittlin, P. J. M. van Bentum, V. H. M. Duijn, and A. A. Menovsky, Phys. Rev. B **51**, R12 049 (1995).
[31] Y. Matsuda, M. B. Gaifullin, K. Kumagai, K. Kadowaki, and T. Mochiku, Phys. Rev. Lett. **75**, 4512 (1995).
[32] In Refs. 19 and 5, the value of $s=1.32$ nm was used. Note that this is length of the unit cell along the *c*-axis; the distance between the neighboring CuO_2 planes is half of that. We thank L. Bulaevskii for pointing that out.
[33] N.-C. Yeh, Phys. Rev. B **43**, 523 (1991).
[34] J. I. Gittleman and B. Rosenblum, Phys. Rev. Lett. **16**, 734 (1966).
[35] A. M. Clogston, Phys. Rev. Lett. **3**, 266 (1962).
[36] B. S. Chandrasekhar, Appl. Phys. Lett. **1**, 7 (1962).
[37] R. A. Smith and V. Ambegaokar, Phys. Rev. B **45**, 2463 (1992).
[38] D. N. Basov, T. Timusk, B. Dabrowski, and J. D. Jorgensen, Phys. Rev. B **50**, R3511 (1994).
[39] M. Dumm, D. N. Basov, Seiki Komiya, Yasushi Abe, and Yoichi Ando, Phys. Rev. Lett. **88**, 147003 (2002).
[40] M. Dumm and D. N. Basov (private communication).
[41] J. J. Tu and C. C. Homes (private communication).
[42] S. A. Kivelson, I. P. Bindloss, E. Fradkin, V. Oganesyan, J. M. Tranquada, A. Kapitulnik, and C. Howald, Rev. Mod. Phys. **75**, 1201 (2003), and references therein.
[43] S. V. Dordevic, S. Komiya, Y. Ando, and D. N. Basov, Phys. Rev. Lett. **91**, 167401 (2003).
[44] B. Nachumi, A. Keren, K. Kojima, M. Larkin, G. M. Luke, J. Merrin, O. Tchernyshov, Y. J. Uemura, N. Ichikawa, M. Goto, and S. Uchida, Phys. Rev. Lett. **77**, 5421 (1996).
[45] A. T. Savici, Y. Fudamoto, I. M. Gat, T. Ito, M. I. Larkin, Y. J. Uemura, G. M. Luke, K. M. Kojima, Y. S. Lee, M. A. Kastner, R. J. Birgeneau, and K. Yamada, Phys. Rev. B **66**, 014524 (2002).
[46] P. M. Singer, A. W. Hunt and T. Imai, cond-mat/0302078.
[47] A proposed picture of intermediate-scale ($\simeq 100-200$ Å) phases separation is reminiscent of the "swiss cheese" model[44–46] put forward to elucidate the impact of Zn doping on the superconducting states properties of YBCO.
[48] H. Kimura, K. Hirota, H. Matsushita, K. Yamada, Y. Endoh, S.-H. Lee, C. F. Majkrzak, R. Erwin, G. Shirane, M. Greven, Y. S. Lee, M. A. Kastner, and R. J. Birgeneau, Phys. Rev. B **59**, 6517 (1999).
[49] M. Fujita, K. Yamada, H. Hiraka, P. M. Gehring, S. H. Lee, S. Wakimoto, and G. Shirane, Phys. Rev. B **65**, 064505 (2002).
[50] D. P. Arovas, A. J. Berlinsky, C. Kallin, and S.-C. Zhang, Phys. Rev. Lett. **79**, 2871 (1997).
[51] C. Panagopoulos, J. L. Tallon, B. D. Rainford, J. R. Cooper, C. A Scott, and T. Xiang, Solid State Commun. **126**, 47 (2003).